Thin Solid Films 518 (2010) 5169–5172

Contents lists available at ScienceDirect

Thin Solid Films

journal homepage: www.elsevier.com/locate/tsf

Letter

Fully strained low-temperature epitaxy of TiN/MgO(001) layers using high-flux, low-energy ion irradiation during reactive magnetron sputter deposition

Keywords:
Epitaxy
Sputter deposition
Transition metal nitrides

Low-temperature epitaxy (LTE) of high-quality materials is of increasing importance in advanced thin film technology since, among other benefits, it offers the possibility of kinetically quenching strain-induced relaxation in heterolayers, thus inhibiting the generation of dislocations and interface defect incorporation during film growth. In addition, developing an understanding of the mechanisms controlling LTE may provide solutions for the growth of high-quality polycrystalline films in low-thermal-budget applications, while providing insights for developing reaction paths leading to the growth of high-quality functional coatings on flexible polymeric substrates.

The crystalline quality of as-deposited layers is typically increased by raising the film growth temperature T_s, and/or lowering the deposition rate R, to provide adatoms longer mean free paths before capture into permanent sites. However, both tactics can result in decreased throughput as well as other disadvantages including additional contamination, increased dopant migration, interface broadening, surface segregation, and higher thermal contraction stress. Moreover, in some applications, the use of a substrate heater is prohibited due to the requirement of rapid cycling times and/or thermally sensitive substrates.

The most commonly employed approaches to LTE involve the use of plasma-assistance during chemical vapor deposition [1,2], physical vapor deposition [3,4], and molecular beam epitaxy [5,6] in which ion-induced gas phase and surface chemistry, together with momentum transfer to the growing film, are thought to play significant roles. In the present experiments, we seek to isolate the effect of low-energy ion bombardment in investigating TiN LTE in which the ions are only nitrogen (to avoid stress associated with trapped Ar ions) with energies below the bulk lattice atom displacement in TiN [7] and for which previous experiments have shown as-deposited polycrystalline and epitaxial films to be stoichiometric with no trapped N [8–11].

Hultman et al. [12,13] investigated the microstructural evolution of TiN films deposited on MgO(001) by reactive magnetron sputter deposition in pure N_2 discharges under conditions similar to those used here (other than the use of high intensity, low-energy ion irradiation) as a function of T_s. The results show that at low T_s (<500 °C) with no intentional ion bombardment, the films are polycrystalline, underdense, and exhibit a pronounced columnar morphology. The substrate potential in those experiments was −17 V giving rise to an incident N_2^+ to Ti flux ratio, $J_{N_2^+}/J_{Ti}$, of ≃1. At T_s ≃500 °C, near the transition from polycrystalline to epitaxial, the films have a high density of low-angle grain boundaries and consist of columnar grains separated by threading dislocations. Layers grown at elevated temperatures (550<T_s<850 °C) are epitaxial, but fully relaxed [14]. TiN/MgO(001) layers, with nearly the same thickness as in the present experiments and grown at T_s = 700 °C under the same deposition conditions, but with $J_{N_2^+}/J_{Ti} = 4$, were also found to be fully relaxed with a misfit density of $\simeq 5\times10^5$ cm^{-2} [15].

Here, we report the results of an investigation of TiN LTE on MgO (001), in the absence of applied substrate heating, using low-energy ($E_{N_2^+}$≃20 eV: 10 eV per incident accelerated N), very high-flux ($J_{N_2^+}/J_{Ti}$≃14) ion irradiation. To this purpose, we employ ultrahigh vacuum (UHV) magnetically-unbalanced [16] reactive magnetron sputter deposition in pure N_2. A pair of external Helmholtz coils, with Fe pole pieces, is used to create a uniform axial magnetic field B_{ext} in the region between the target and the substrate and, hence, unbalance the magnetic circuit associated with the permanent magnets in the magnetron source. This has the effect of focusing the discharge to greatly increase the plasma density near the substrate without significantly affecting the target sputtering rate [16]. The ion flux is controlled by B_{ext} and the ion energy is set by eV_s, where V_s is the sum of the applied substrate potential and the plasma potential [8].

TiN layers, 0.3 μm thick, are grown on electrically-floating substrates in a load-locked UHV system [8] from a 99.999% pure Ti target in N_2 (99.999%) at 20 mTorr (2.67 Pa) with a target-to-substrate separation of 6.5 cm. The relatively large pressure is used to suppress kinetic energy transfer to the growing film by fast sputtered atoms and energetic ions which are neutralized and backscattered from the target [17]. Thus, the primary energetic species incident at the growing film are ions, accelerated across the anode sheath, which are essentially monoenergetic since the charge-exchange mean free path [18] is more than 10× larger than the sheath width [19]. The composition of the ion flux at the substrate under the present set of growth conditions is 96.3% N_2^+, 3.5% N^+, and 0.2% Ti^+ as determined by high-resolution mass spectroscopy measurements [20].

A combination of Langmuir probe, deposition rate, and film composition measurements show that the ion-to-metal ratio $J_{N_2^+}/J_{Ti}$ incident at the growing film is 14 with $E_{N_2^+} = eV_s \simeq 20$ eV (i.e., ≃10 eV per N following collisionally-induced dissociation). The deposition rate R is 2.5 Å s^{-1}.

The substrates are polished $10\times10\times0.5$ mm^3 MgO(001) wafers which are cleaned and degreased by successive rinses in ultrasonic baths of trichloroethane, acetone, methanol, and de-ionized water and blown dry in dry N_2. Final substrate cleaning consists of thermal degassing at 500 °C for one hour in UHV. Following degassing, the substrates are allowed to cool to room temperature. Immediately prior to initiating deposition, the Ti target is sputter etched for 5 min with a shutter shielding the substrate. The film growth temperature T_s due to plasma heating was measured by a thermocouple bonded to a dummy TiN-coated MgO substrate. T_s increased from room temperature to 50 °C during sputter-cleaning of the target, then increased approximately linearly to 320 °C during the first 100 s of deposition followed by a shallow linear rise to 420 °C at the end of the 20 min deposition period.

We choose to use a floating substrate potential during film growth in order to minimize the ion energy, and hence ion irradiation-induced film damage, while providing significant momentum

doi:10.1016/j.tsf.2010.04.028

transfer, due to the very high ion/metal flux ratio, to adatoms during the early stages of film growth on an electrically insulating substrate. That is, at the floating potential, there is no net current; the ion current is precisely balanced by the electron current. Thus, the ion flux to the growing film is constant throughout growth, from the earliest stages of film nucleation, which is crucial for low-temperature epitaxial growth.

The stoichiometry of as-deposited films is determined using 2 MeV He^+ Rutherford backscattering spectroscopy (RBS); the spectra is analyzed with the RUMP simulation program [21]. All TiN layers are stoichiometric with an uncertainty in measured N/Ti ratios of less than ± 0.02. Film nano- and micro- structures are analyzed using a combination of x-ray diffraction (XRD) and transmission electron microscopy (TEM). A high-resolution Philips MRD diffractometer, with a Cu K_α source ($\lambda = 1.540597$ Å) and a four-crystal Ge(220) monochromator, is used for the XRD measurements. A two-crystal Ge (220) analyzer placed in front of the detector provides an angular divergence of <12 arc-s with a wavelength spread $\Delta\lambda/\lambda \simeq 7\times10^{-5}$. TEM and high-resolution cross-sectional TEM (HR-XTEM) analyses are performed using Philips CM-12 and Hitachi H9000 microscopes operated at 120 and 300 kV, respectively. TEM and XTEM specimen preparation followed the procedure described in Ref. [22].

Only one film peak is observed in high-resolution XRD (HR-XRD) ω–2θ scans from TiN/MgO(001) layers grown with no applied substrate heating. Fig. 1(a) shows a narrow region of a typical scan. The peaks centered at 42.466° and 42.917° are indexed as 002 TiN and MgO, respectively. From the known lattice constant of MgO, $a_{MgO} = 0.42112$ nm [23], and the measured angular separation $\Delta 2\theta$ between the substrate and layer peaks, 0.451°, the lattice parameter along the film growth direction of as-deposited TiN is determined to be 0.42539 nm. This value is 0.33% larger than the reported bulk TiN lattice constant, $a_{TiN} = 0.4240$ nm [24], showing that the film exhibits weak in-plane compression. The TiN 002 diffraction peak has a full width at half maximum intensity $\Gamma_{2\theta} = 0.05°$. The inset in Fig. 1(a) is a TiN 002 ω-rocking curve with $\Gamma_\omega = 0.13°$.

In-plane and perpendicular x-ray coherence lengths $\xi_{||}$ and $\xi_\perp$ were determined from the widths of the 002 diffracted intensity distributions perpendicular $\Delta g_\perp$ and parallel $\Delta g_{||}$, respectively, to the diffraction vector $\overline{g}$ using the relationships [25]

$$\xi_{||} = 2\pi / |\Delta g_\perp| = \lambda / [2\Gamma_\omega \sin\theta] \quad (1)$$

and

$$\xi_\perp = 2\pi / |\Delta g_{||}| = \lambda / [\Gamma_{2\theta} \cos\theta]. \quad (2)$$

In Eqs. (1) and (2), Γ_ω and $\Gamma_{2\theta}$ are the full widths at half maximum intensities of the 002 Bragg peak in the ω and 2θ directions, respectively. From the data presented in Fig. 1, $\xi_{||}$, a measure of the lateral film mosaicity, is 94 nm, and $\xi_\perp$, limited by both the film thickness and vertical mosaicity, is 190 nm. In comparison, $\xi_{||} = 86$ nm and $\xi_\perp = 140$ nm for 0.26-μm-thick TiN(001) layers grown at $T_s = 700$ °C [15]. Thus, the LTE TiN(001) layers grown with no applied substrate heating are comparable to those grown at 700 °C. That is, the present films exhibit high crystalline quality with low mosaicity.

A typical LTE TiN/MgO(001) HR-XRD ϕ scan, obtained in the parallel-beam mode with ω and 2θ angles set to detect the 220 peaks at a tilt angle of 45° with respect to the surface normal, is presented in Fig. 1(b). The results show four 90°-rotated 220 peaks at the same ϕ angles for both TiN and MgO. The combination of the HR-XRD ω–2θ and ϕ scans demonstrate that our TiN(001) layers grow epitaxially with a cube-on-cube relationship to the substrate: $(001)_{TiN}||(001)_{MgO}$ and $[100]_{TiN}||[100]_{MgO}$.

In-plane $a_{||}$, out-of-plane $a_\perp$, and relaxed a_o lattice parameters of as-deposited TiN(001) layers are determined from high-resolution reciprocal lattice map (HR-RLM) results. Reciprocal lattice maps about the asymmetric 113 reflection are shown in Fig. 2 for both (a) LTE TiN(001) and, for comparison, (b) an epitaxial TiN(001) layer with essentially the same thickness, grown at 700 °C. [15] Diffracted intensity distributions are plotted as isointensity contours as a function of the reciprocal lattice vectors $k_{||}$ parallel and $k_\perp$ perpendicular to the surface.[26] For a 113 reflection from a 001-oriented NaCl-structure sample, $a_{||} = \sqrt{2}/k_{||}$ and $a_\perp = 3/k_\perp$. From the HR-RLMs in Fig. 2, we obtain $a_{||} = 0.42162$ nm and $a_\perp = 0.42506$ nm for the LTE TiN (001) layer with $a_{||} = 0.42289$ nm and $a_\perp = 0.42458$ nm for the 700 °C TiN(001) layer. Relaxed bulk TiN(001) lattice parameters a_o were determined from $a_{||}$ and $a_\perp$ values through the relationship [15]:

$$a_o = a_\perp \left(1 - \frac{2\nu\left(a_\perp - a_{||}\right)}{a_\perp(1+\nu)}\right). \quad (3)$$

Using Eq. (3), a_o for the LTE TiN(001) layer is found to be 0.42386 nm, in good agreement with the value 0.42397 nm obtained for the 700 °C TiN(001) layer.

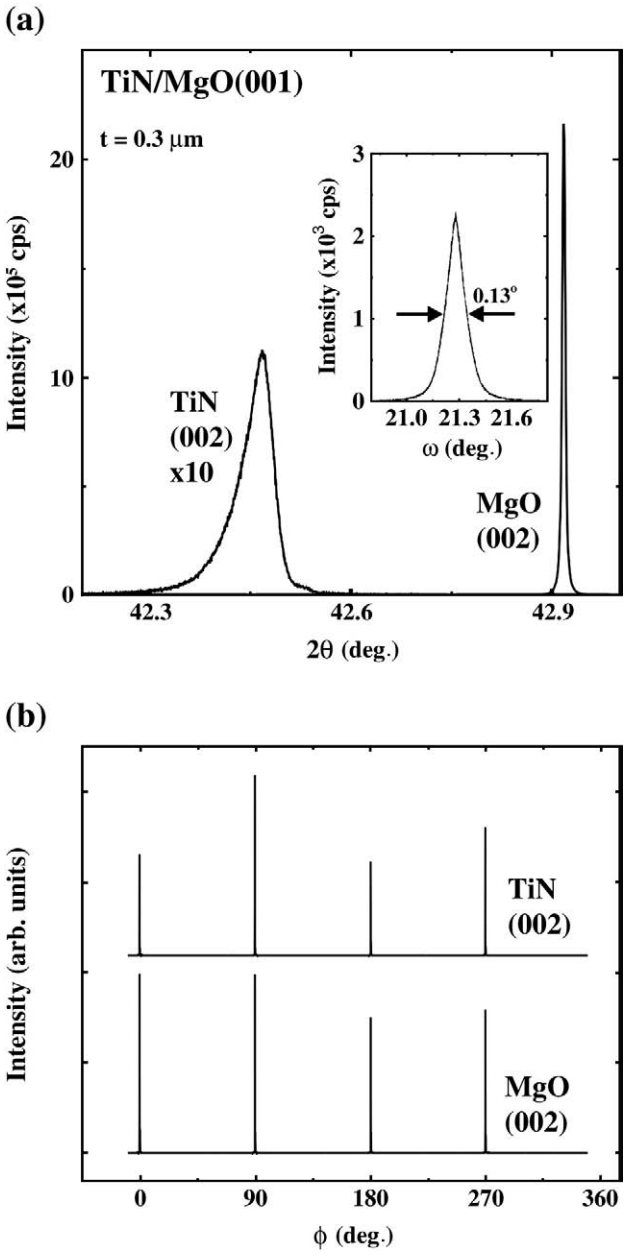

Fig. 1. (a) HR-XRD ω–2θ scan, and a 002 ω-rocking curve (inset), from a 0.3-μm-thick LTE TiN layer grown on MgO(001) with $J_i/J_{Ti} = 14$ and $E_i \simeq 20$ eV. (b) TiN and MgO XRD 220 ϕ-scans from the sample corresponding to (a).

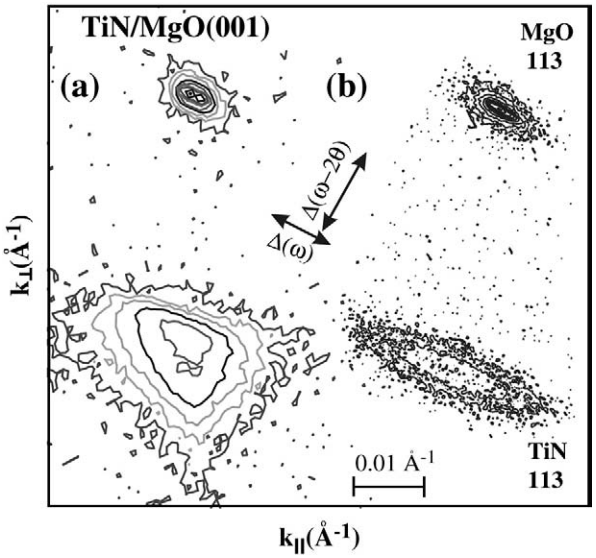

Fig. 2. HR-RLMs around the 113 reflection of TiN layers grown on MgO(001): (a) LTE and (b) $T_s = 700$ °C.

The fact that the substrate and layer peaks for the LTE TiN(001) film [Fig. 2(a)] are aligned along $k_{||}$ to within the instrument detection limit, $\simeq 5\times10^{-4}$ Å^{-1}, indicates that the film is fully strained. In contrast, substrate and layer peaks of the 700 °C TiN(001) layer are misaligned along $k_{||}$, revealing the presence of in-plane-strain relaxation due to misfit dislocations. As reported in [15], the residual strain, $\varepsilon_{||} = -0.26\%$, can be accounted for by differential contraction during sample cooling following deposition at 700 °C. The thermal expansion coefficients of TiN and MgO are $9.35\times10^{-6}\,K^{-1}$ [27] and $1.3\times10^{-6}\,K^{-1}$ [28], resulting in a thermal strain of −20%, which is equal, within experimental uncertainty, to the measured strain. Therefore, the 700 °C TiN(001) film is fully relaxed at the growth temperature.

Fig. 3 is a typical HR-XTEM image, obtained along the [100] zone axis, from an LTE TiN/MgO(001) layer. The darker contrast of the TiN film compared to the MgO substrate is due to the mass difference between Ti (47.9 amu) and Mg (24.3 amu). The lattice fringes are continuous across the film/substrate interface, consistent with the XRD results showing that the layer has a cube-on-cube epitaxial relationship to the substrate. The absence of misfit dislocations in both HR and lower-resolution XTEM images is in agreement with the HR-RLM data in Fig. 2(a). The dark regions in the XTEM image are due to local strain fields associated with lattice defects. Some of these defects are the result of Ar^+-ion milling during XTEM specimen preparation. This is certainly the case for local strain fields observed within the substrate. However, the number density of strain fields is larger in the film indicating that defects form at the film surface during growth, but threading dislocations are inhibited, via kinetic restrictions, from gliding to the interface due to the low deposition temperatures. XTEM images and HR-RLM results provide clear evidence that the interface is free of misfit dislocations.

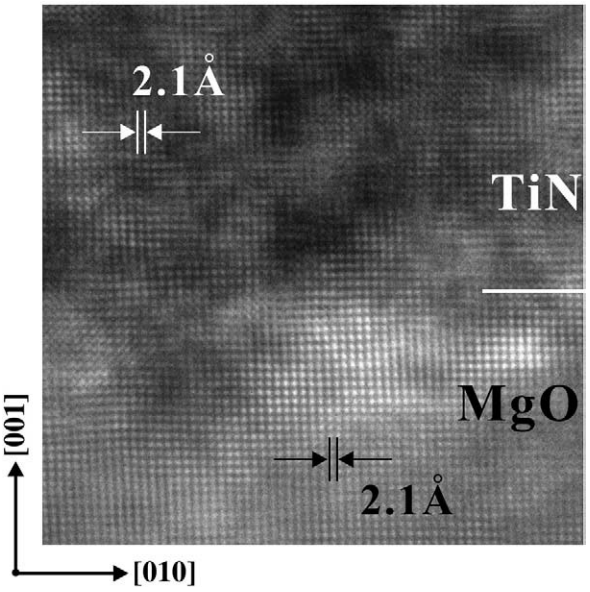

Fig. 3. A HR-XTEM image, along the [100] zone axis, from an LTE TiN layer grown on MgO(001) with $J_i/J_{Ti} = 14$ and $E_i \simeq 20$ eV.

The combined HR-XRD and HR-XTEM results demonstrate that LTE TiN layers grown using high-flux, low-energy ion irradiation exhibit high crystalline quality with low mosaicity and are fully strained with no detectable misfit dislocations. The low growth temperatures used in these experiments kinetically quench interfacial relaxation due to dislocation nucleation and glide, while epitaxial TiN layers, with equivalent thicknesses, grown at 700–850 °C are fully relaxed with misfit dislocation densities of $\simeq 5\times10^{-5}\,cm^{-2}$. We note that while the maximum growth temperature during LTE is 420 °C ($T_s/T_m \sim 0.2$, where T_m is the TiN melting point, 3203 K [29]), the first 250 Å are grown at $T_s < 320$ °C. More importantly, nucleation and the early stages of film growth take place at temperatures < 100 °C ($T_s/T_m \simeq 0.1$) under conditions in which each surface cation experiences collisions with multiple 10 eV N particles before being incorporated into a "bulk" lattice site. The impact energy per incident fast N, $E_i \simeq 10$ eV, is too low for significant lattice penetration. Thus, most of the momentum transfer is efficiently coupled to the surface.

In conclusion, we have demonstrated that epitaxial TiN/MgO(001) layers can be grown in the absence of applied substrate heating using very high flux, low-energy (below the lattice atom displacement threshold), ion irradiation during reactive magnetron sputter deposition. HR-XRD and HR-TEM analyses reveal that the TiN(001) layers grow with an $(001)_{TiN}||(001)_{MgO}$ and $[100]_{TiN}||[100]_{MgO}$ orientation relationship to the substrate and are fully coherent with no detectable misfit dislocations. For comparison, TiN layers grown at temperatures of 700–850 °C under similar conditions, but with no intentional ion irradiation, are fully relaxed with a high misfit dislocation density. Thus, the present results reveal that intense low-energy ion irradiation during film growth facilitates high adatom mobilities giving rise to low-temperature epitaxy, while the low growth temperature quenches strain-induced relaxation and suppresses misfit dislocation formation.

Acknowledgments

This research was supported by the U.S. Department of Energy, Division of Materials Science, grant DEFG02-91ER45439 through the University of Illinois Frederick Seitz Materials Research Laboratory (FS-MRL) and by Priority Research Centers Program through the National Research Foundation of Korea (NRF) funded by the Ministry of Education, Science and Technology (2009-0093823). We appreciate the use of the facilities at the FS-MRL Center for Microanalysis of Materials, which is partially supported by DOE, at the University of Illinois.

References

[1] S. Cereda, F. Zipoli, M. Bernasconi, Leo Miglio, F. Montalenti, Phys. Rev. Lett. 100 (2008) 046105.
[2] T. Kitagawa, M. Kondo, A. Matsuda, Appl. Surf. Sci. 159 (2000) 30.
[3] K.C. Ruthe, D.J. Cohen, S.A. Barnett, J. Vac. Sci. Technol. A 22 (6) (2004) 2446.
[4] N.-E. Lee, G.A. Tomasch, J.E. Greene, Appl. Phys. Lett. 65 (25) (1994) 3236.
[5] S.H. Park, H. Suzuki, T. Minegishi, G. Fujimoto, J.S. Park, I.H. Im, D.C. Oh, M.W. Cho, T. Yao, J. Crystal Growth 309 (2007) 158.

[6] S. Kimura, S. Emura, Y. Yamauchi, Y.K. Zhou, S. Hasegawa, H. Asahi, J. Crystal Growth 310 (2008) 40.
[7] I. Petrov, L. Hultman, J.-E. Sundgren, J.E. Greene, J. Vac. Sci. Technol. A 10 (1992) 265.
[8] F. Adibi, I. Petrov, J.E. Greene, L. Hultman, J.-E. Sundgren, J. Appl. Phys. 73 (1993) 8580.
[9] B.W. Karr, D.G. Cahill, I. Petrov, J.E. Greene, Phys. Rev. B 61 (2000) 16137.
[10] C.-S. Shin, D. Gall, N. Hellgren, J. Patschieder, I. Petrov, J.E. Greene, J. Appl. Phys. 93 (2003) 6025.
[11] T. Lee, K. Ohmori, C.-S. Shin, D.G. Cahill, I. Petrov, J.E. Greene, Phys. Rev. B 71 (2005) 144106.
[12] L. Hultman, G. Hakansson, U. Wahlstrom, J.-E. Sundgren, I. Petrov, F. Adibi, J.E. Greene, Thin Solid Films 205 (1991) 153.
[13] L. Hultman, U. Helmersson, J.-E. Sundgren, J.E. Greene, J. Appl. Phys. 61 (1987) 552.
[14] L. Hultman, S.A. Barnett, J.E. Sundgren, J.E. Greene, J. Cryst. Growth 92 (1998) 639.
[15] C.-S. Shin, S. Rudenja, D. Gall, N. Hellgren, T.-Y. Lee, I. Petrov, J.E. Greene, J. Appl. Phys. 95 (2004) 356.
[16] I. Petrov, F. Adibi, J.E. Greene, W.D. Sproul, W.-D. Münz, J. Vac. Sci. Technol. A 10 (1992) 3283.
[17] J.E. Greene, J.-E. Sundgren, L. Hultman, I. Petrov, D.B. Bergstrom, Appl. Phys. Lett. 67 (1995) 2928.
[18] A.V. Phelps, J. Phys. Chem. Ref. Data 20 (1991) 557.
[19] B. Chapman, Glow Discharge Processes, Wiley, New York, 1980, p. 108.
[20] I. Petrov, A. Myers, J.E. Greene, J.R. Abelson, J. Vac. Sci. Technol. A 12 (1994) 2846.
[21] R.L. Doolittle, Nucl. Instrum. Methods Phys. Res. B 15 (1985) 344.
[22] J.-P. Noel, N. Hirashita, L.C. Markert, Y.-W. Kim, J.E. Greene, J. Knall, W.-X. Ni, M.A. Hasan, J.-E. Sundgren, J. Appl. Phys. 65 (1989) 1189.
[23] Inorganic Index to Powder Diffraction File (Joint Committee on Powder Diffraction Standards, Swarthmore, PA, 1997): Card No. 45-0946.Swarthmore, PA, 1997): Card No. 45-0946.
[24] Inorganic Index to Powder Diffraction File (Joint Committee on Powder Diffraction Standards, Swarthmore, PA, 1997): Card No. 45-0946.Swarthmore, PA, 1997): Card No. 38-1420.
[25] R.C. Powell, N.-E. Lee, Y.-W. Kim, J.E. Greene, J. Appl. Phys. 73 (1998) 189.
[26] P. van der Sluis, J. Phys. D 26 A (1993) 188.
[27] K. Aigner, W. Lengauer, D. Rafaja, P. Ettmayer, J. Alloys Compd. 215 (1994) 121.
[28] H. Landolt, R. Börnstein, Numerical Data and Functional Relationships in Science and Technology, Goup III, vol. 7, Pt. b1, Springer, Berlin, 1975, p. 27.
[29] H.O. Pierson, Handbook of Refractory Carbides and Nitrides: Properties, Characteristics, Processing, and Applications, William Andrew, New Jersey, 1996 p. 193.

Taeyoon Lee
Nano Bio Fusion Device Laboratory, School of Electrical and Electronic Engineering, Yonsei University, 134 Shinchon-dong, Seodaemun-gu, Seoul 120-749, Republic of Korea

H. Seo
H. Hwang
B. Howe
Department of Materials Science and the Fredrick Seitz Materials Research Laboratory University of Illinois, 104 South Goodwin, Urbana, IL 61801, United States

S. Kodambaka
Department of Materials Science and Engineering, University of California Los Angeles, Los Angeles, CA 90095, United States

J.E. Greene
I. Petrov*
Department of Materials Science and the Fredrick Seitz Materials Research Laboratory University of Illinois, 104 South Goodwin, Urbana, IL 61801, United States
*Corresponding author.
E-mail address: petrov@illinois.edu (I. Petrov).

3 March 2010